Topics in Catalysis (2022) 65:1573–1586
https://doi.org/10.1007/s11244-021-01514-0

ORIGINAL PAPER

Vibrational Properties of CO Adsorbed on Au Single Atom Catalysts on TiO_2(101), ZrO_2(101), CeO_2(111), and $LaFeO_3$(001) Surfaces: A DFT Study

Ho Viet Thang[1,2] · Farahnaz Maleki[2] · Sergio Tosoni[2] · Gianfranco Pacchioni[2]

Accepted: 23 September 2021 / Published online: 14 December 2021

Abstract

The nature and local environment of Au single atoms supported and stabilized on four different oxides is studied by means of DFT + U calculations using CO as probe molecule and its stretching frequency, ω_e, as a fingerprint of the site where the Au atom is bound. Four oxides are considered, anatase TiO_2, tetragonal ZrO_2, cubic CeO_2, and a perovskite $LaFeO_3$. In this latter case a recently reported experimental study has detected a stretching mode for CO adsorbed on $Au_1/LaFeO_3$ of 2215 cm^{-1}, with a large blue shift, $\Delta\omega(CO) = 72$ cm^{-1} with respect to free CO. In order to identify the Au adsorption site that can give rise to this large blue-shift we have considered five cases: (a) Au replacing a lattice cation, $(Au)_{subM}$; (b) Au replacing a lattice O anion, $(Au)_{subO}$; (c) Au adsorbed on the surface, $(Au)_{ads}$; (d) Au bound to an extra O atom on the surface, $(AuO)_{ads}$, or (e) Au bound to two extra O atoms on the surface, $(AuO_2)_{ads}$. It turns out that the correct reproduction of $\Delta\omega$ for CO adsorbed on positively charged gold, $Au^{\delta+}$, is challenging for DFT. Therefore, we have performed a comparative study of $Au^{\delta+}$-CO molecular compounds for which $\omega_e(CO)$ is known experimentally using various kinds of DFT functionals and accurate CCSD and CCSD(T) quantum chemistry methods. Also based on this comparison we propose a tentative assignment for the observed frequency of CO adsorbed on $Au_1/LaFeO_3$ single atom catalyst.

Graphic Abstract

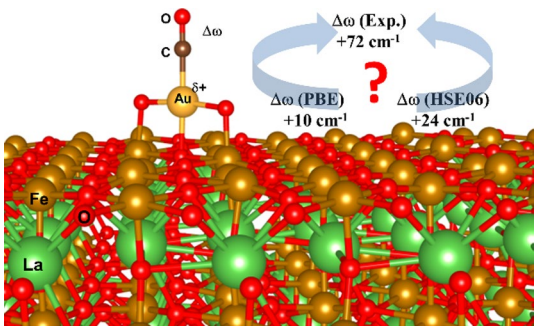

Keywords Single atom catalysis · Oxide surfaces · Au-CO molecular complexes · CO vibrational frequency · Density functional theory

1 Introduction

Single atom catalysts (SAC) are emerging as a novel and promising class of heterogeneous catalysts [1, 2]. A number of interesting features makes them attractive for fundamental studies of the relationships between structure and properties. Being the result of the deposition

✉ Gianfranco Pacchioni
gianfranco.pacchioni@unimib.it

1 The University of Danang, University of Science and Technology, Danang 550000, Vietnam

2 Dipartimento di Scienza dei Materiali, Università di Milano-Bicocca, via Cozzi 55, 20125 Milan, Italy

and stabilization of an isolated transition metal atom on a support, SACs have a lot in common with coordination compounds, where a transition metal atom or cation is surrounded by organic ligands [3]. In a sense, the support in SACs can be viewed as a very bulky ligand. The presence of a single active site is another characteristic of SACs that can be particularly interesting to increase the selectivity of catalytic reactions. SACs have the advantage that they can be prepared with tiny amounts of precious metals, thus reducing costs and increasing the overall efficiency of the catalyst. Another aspect that makes these systems attractive is that SACs can be deposited on virtually any solid material, oxides, carbides, carbon-based materials, zeolites, etc., opening in principle the possibility to tune the activity of the catalyst in a desired way. It is not surprising that the number of papers dedicated to SACs has increased enormously in the last decade.

We mentioned above the similarity of SACs with homogenous catalysts based on transition metal complexes [3]. In both cases the active site is a single metal atom, and in both cases the activity can be modified and sometimes modulated by changing the "surrounding" (either the support or the ligands). Beside this obvious similarity, there is also a substantial difference between SACs and coordination compounds. This is the level of definition and characterization of the active site. In homogeneous catalysis the metal complex that forms the active phase can be isolated and structurally characterized so that a precise and complete knowledge is obtained about the structure; things are much more complex for SACs. On every support there are several sites where the metal atoms can be stabilized; these can replace lattice ions (both cations or anions, and in this case they should be referred to as "dopants"), be adsorbed near surface defects or attached to functional groups, or even incorporated in voids, structural holes, morphological defects in the support. The situations can be very different if the support is an oxide or a carbon-based material. In the first case the metal atoms can be stabilized at steps, corners, kinks, near OH groups, attached to impurity atoms, etc.; in the second case a great variety of supports has been used going from graphene to graphene-oxide, from N-doped graphene to C_3N_4, etc. Furthermore, there is increasing evidence that SACs are not static but are dynamic objects that can change their position according to the reaction conditions, for instance depending on the oxidizing or reducing nature of the reaction environment [4].

The lack of precise information about the structural nature and local coordination of SACs is a serious problem for the theoretical rationalization of the catalytic behavior using electronic structure methods (e.g. based on density functional theory, DFT). In fact, to reproduce or predict the activity of a given SAC a well-defined structural model must be provided as input of the calculation. This choice is very delicate as completely different results can be obtained when the active metal site is in different local environments.

Recently we have studied the nature of isolated Rh, Ru and Pt species deposited on two representative oxide surfaces, anatase TiO_2 (a reducible oxide), and tetragonal ZrO_2 (a non-reducible oxide) [5–9]. These systems have been characterized experimentally using high-resolution scanning transmission electron microscopy (STEM), Fourier transform infrared spectroscopy (FTIR), and temperature programmed desorption (TPD) spectra of adsorbed CO probe molecules. Combining these data with extensive DFT calculations it has been possible to provide a realistic and sometimes unambiguous identification of the stable single-atom species present on these supports. In many cases it emerges that the Rh, Ru or Pt atoms are bound to O atoms on the surface due to the presence of OH groups; the interaction of the metal atoms with the OH groups result in MO or MO_2 surface complexes where the metal atom is in positive oxidation state [5–9]. The identification has been largely based on the comparison of measured and computed CO stretching frequencies and frequency shifts, $\Delta\omega$. Using scaling factors for the frequencies, it has been possible to quantitatively reproduce the vibrational frequency of the real SACs, an essential step for the complete identification of their structural nature [4–9].

Thus, CO probe molecules can provide a way to assess the nature and coordination of a SAC, provided that experimental CO vibrational properties are available (and possibly adsorption strength as derived from TPD or other measurements); combining this information with the corresponding computed data can provide a way to distinguish among various possible environments for SAC in static conditions [5]. The scope of this paper is to use this procedure to identify the nature of a recently reported Au SAC, $Au_1/LaFeO_3$ for which the vibrational frequency of adsorbed CO has been reported, showing a particularly large positive shift, Fig. 1 [10].

The nature of Au SACs on $LaFeO_3$ has been compared with that of Au atom supported on anatase TiO_2, tetragonal ZrO_2, and cubic CeO_2. For these systems, however, the experimental information is lacking or less specific. The choice is dictated by the desire to compare reducible ($LaFeO_3$, TiO_2, CeO_2) with non-reducible (ZrO_2) oxides, and to consider some of the most widely used oxides as supports for SACs.

We will show that the calculation of the vibrational properties of CO adsorbed on a Au atom in positive oxidation state presents considerable problems for theory, and for this reason we will first benchmark our approach by comparing the measured and computed properties of CO adsorbed on a series of $Au^{\delta+}$-CO molecular complexes using methods based both on DFT and on wave function determination (quantum chemistry approaches). In this way we will be able

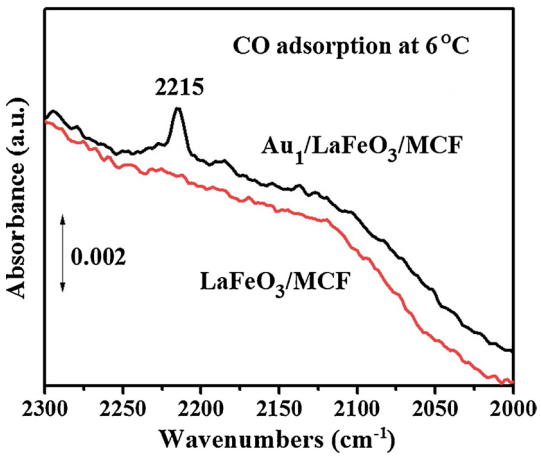

Fig. 1 FTIR spectra of CO adsorption on the $LaFeO_3$ and Au_1/$LaFeO_3$. The spectra show the appearance of a new peak due to CO adsorption when Au is atomically dispersed on the surface. Reproduced with permission from ref. [10]

to assess the reliability of the computed CO vibrational frequencies, and to compare the results with experiment.

The paper is organized as follows. In Sect. 2 we provide the details of the molecular and solid-state periodic calculations performed on Au-containing molecular complexes and on oxide supports, respectively. Section 3 reports the results and is divided in the same way: Sect. 3.1 contains the molecular results; Sect. 3.2 reports the data for CO adsorption on Au atoms in various environments of the four oxides considered. The Conclusions are summarized in the last Section.

2 Computation Methods and Models

In this work we have studied both molecular systems and crystalline solids. Thus, two different computational approaches and electronic structure codes have been used. For the study of Au molecular complexes we used the Gaussian code [11] making use of local gaussian-type atomic orbital basis sets; for the study of oxide surfaces and Au SACs we adopted the periodic VASP code [12] based on plane wave and supercell approaches.

2.1 Molecular Calculations

A series of Au containing simple molecular complexes has been studied at various theoretical levels. Both DFT and high-quality quantum chemistry methods (coupled-cluster, CC) have been used. All the calculations have been performed by means of the Gaussian-16 package [11]. The geometries of all gas-phase species were fully optimized with the def2-TZVPPD Weigend–Ahlrichs basis set [13]. For the Au atom, we used a relativistic small-core effective core potential (ECP), treating 5s, 5p, 5d and 6s states explicitly [14]. In order to obtain a benchmark of the stretching frequency of CO bound to Au in positive oxidation state the following methods have been used: two standard DFT functionals (PBE [15] and M06L [16]), four hybrid functionals (HSE06 [17], M06 [18], M06-2X [18], M06-HF [19], and the coupled-cluster method including single-double (CCSD) and single-double-triple (CCSD(T)) [20] excitations. In all cases harmonic vibrational frequencies have been computed; the frequencies reported for the molecular calculations are not scaled. The binding energies of CO, $E_{X\text{-}CO}$, are computed by the difference between isolated species and the CO complexes. A stable complex corresponds to a positive value of the adsorption energy.

2.2 Supercell Calculations

Spin-polarized DFT calculations using the Perdew-Burke-Ernzerhof (PBE) exchange–correlation functional [15] have been performed employing the VASP code [12]. For a specific single case also a HSE06 [17] calculation has been performed (see below). The interactions between core electrons and nuclei are described by the projector-augmented wave (PAW) method [21, 22]; the following valence electrons are treated explicitly: Fe(3p, 3d, 4s), Ti(3p, 3d, 4s), Zr(4s, 4p, 4d, 5s), Ce(4f, 5s, 5p, 5d, 6s), La(5s, 5p, 5d, 6s), O(2s, 2p), C(2s, 2p), Au(5d, 6s). In the case of Au, we adopt a larger core pseudopotential (11 valence electrons) compared to the molecular case (19 valence electrons), as this is the only available option for Au in the PAW library. This is not expected to cause any major deviation on the calculated results [23].

To partly correct the error of on-site Coulomb interactions of transition metals in the PBE method, a Hubbard U parameter has been used for the following elements: U = 4 eV for 3d Fe [24], U = 4.5 eV for 4f Ce [25], U = 4 eV for 4d Zr [26], and U = 3 eV for 3d Ti [26]. Different from TiO_2, ZrO_2 and CeO_2 materials, a wide range of U parameters (from 4 to 8 eV) has been used for $LaFeO_3$ [27]. We used U = 4 eV for Fe because with this value the cell parameters and band gap of bulk $LaFeO_3$ are reproduced reasonably well. In particular, the calculated (in parenthesis experimental [28]) cell parameters are a = 5.557 (5.553) Å, b = 5.647 (5.563) Å, c = 7.912 (7.862) Å and the band gap 2.36 eV (2.34 eV [29]). All magnetic configurations of $LaFeO_3$ have been considered including A-type, C-type, G-type anti-ferromagnetic and ferro-magnetic. The most stable structure is G-type (anti-ferromagnetic) in agreement with previous DFT calculations [24, 30] and experimental studies [31].

A plane-wave basis with a cut-off energy of 400 eV was applied for all calculations. The 1 × 1 × 1 Monkhorst–Pack k-point was applied for Brillouin-zone integration. The

calculations are converged when the electron forces are less than |0.01| eV/Å. The effective charge of atoms is calculated by means of the Bader method [32–34]. The dipole correction along the non-periodic z-direction is also included in all calculations.

The adsorption energies, E_{ads}, of CO are computed as the difference between isolated species and the CO complexes. The stretching frequencies of CO are calculated within the harmonic approximation, in which the CO molecule and the atom directly bound to CO are considered. To compare to the experimental data of CO stretching frequencies, a scaling factor 2143/2125 is used (2143 and 2125 are the CO frequencies of experiment and PBE calculation in gas-phase, respectively).

For $LaFeO_3$(001) surface, a slab of (2 × 2) supercell ($La_{24}Fe_{24}O_{72}$) consisting of six-atomic layers was adopted [35]. For tetragonal ZrO_2(101) and anatase TiO_2(101) surfaces, we used (3 × 1) and (3 × 2) supercells, respectively, of fifteen atomic layers, corresponding to $Ti_{60}O_{120}$ and $Zr_{60}O_{120}$ formula units, respectively. For the CeO_2(111) surface, a (2 × 2) supercell consisting of nine atomic layers, $Ce_{48}O_{96}$, was adopted [25]. In all models, a thickness of vacuum larger than 15 Å is created to minimize the interactions between slabs. The structural models of these materials are shown in Fig. 2a–d.

All adsorption energies are defined positive for bound compounds, $\Delta E_{AB} = -E(AB) + E(A) + E(B)$.

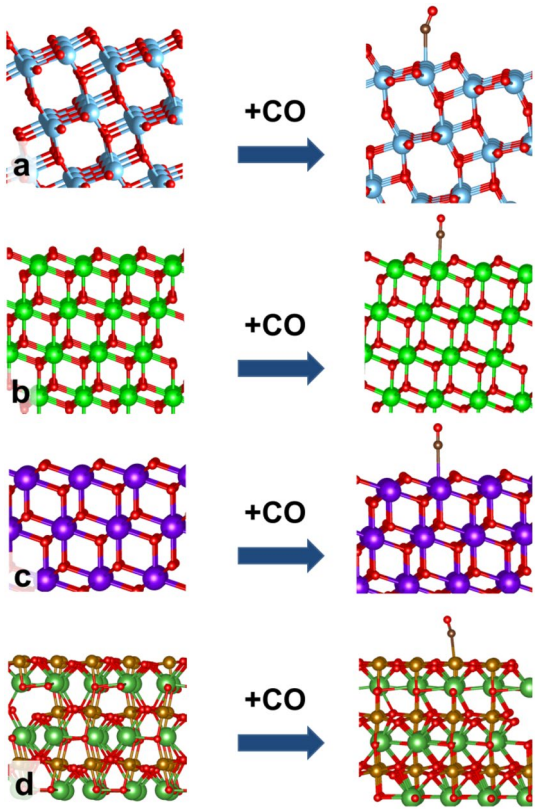

Fig. 2 CO adsorption on the pristine surfaces of **a** TiO_2(101), **b** ZrO_2(101), **c** CeO_2(111) and **d** $LaFeO_3$(001)

3 Results and Discussion

3.1 Au Molecular Complexes

In order to assess the reliability of the method in predicting the CO adsorption properties we have identified a number of simple molecules for which experimental IR spectra are available; these are $[Au\text{-}CO]^+$ [36], Cl-Au-CO and Br-Au-CO (in solution [37]), CF_3-Au-CO [38], and $[L\text{-}Au\text{-}CO]^+$ (L = IDipp] [39] (in the calculations the phenyl ring has been replaced by a methyl group). The list is completed by another set of molecules for which we performed CCSD and CCSD(T) calculations as benchmark, since experimental data are not available: $[Au\text{-}CO]^{2+}$, $[Au\text{-}CO]^{3+}$, and F-Au-CO.

We start from the simplest $[Au\text{-}CO]^+$ complex for which a $\Delta\omega$(CO) of + 94 cm^{-1} has been measured [36], Table 1 Pure DFT functionals, such as PBE or M06L, give very similar results and $\Delta\omega \approx +80$ cm^{-1}, slightly underestimated compared to experiment. Hybrid functionals with about 25% of exact exchange (HSE06 or M06), give very accurate shifts of about 100 cm^{-1} (similar results in terms of equilibrium C-O bond distance and thus presumably also in terms of CO frequency have been previously reported also with B3LYP [40]); increasing the amount of exact exchange (M06-2X or M06-HF) $\Delta\omega$ is slightly overestimated, $\Delta\omega = +109$ cm^{-1} and $\Delta\omega = +121$ cm^{-1}, respectively. Finally, CCSD(T) is also reasonably close to the experiment, $\Delta\omega = +108$ cm^{-1}, while the CCSD method tends to overestimate the shift, Table 1.

The second compound considered, $[L\text{-}Au\text{-}CO]^+$, also carries a net positive charge, partly localized on the Au atom. Here the experimentally measured shift, + 49 cm^{-1} [39], is considerably smaller than in $[Au\text{-}CO]^+$, mainly because the positive charge is partly delocalized. Also in this case PBE underestimates the shift, + 34 cm^{-1}, while HSE06 is in excellent agreement, + 52 cm^{-1}. Unfortunately, we could not obtain CCSD values because the system is too big for our machines. From these results one could conclude that HSE06 is the right method to determine the vibrational shift of CO adsorbed on $Au^{\delta+}$ compounds. However, things are not so simple. In fact, the next step has been to compute the $\Delta\omega$(CO) for two other charged complexes, $[Au\text{-}CO]^{2+}$ and $[Au\text{-}CO]^{3+}$. Here experimental values are not available, and the best estimate is that of CCSD(T) calculations. For $[Au\text{-}CO]^{2+}$, $\Delta\omega$ is 150 cm^{-1} at the CCSD(T) level (+ 171 cm^{-1} at the CCSD level) and the HSE06 value is close, + 164 cm^{-1} (notice that this is considerably underestimated at the PBE level, + 121 cm^{-1}). More complex is the case of Au(III), $5d^8$,

Table 1 Properties of CO adsorbed on Au cations or Au complexes where Au is in positive oxidation state

		Pure DFT		Hybrid DFT				Coupled cluster		Exp.
		PBE	M06-L (0%HF)	HSE06 (25%HF)	M06 (27%HF)	M06-2X (54%HF)	M06-HF (100%HF)	CCSD	CCSD(T)	
CO	ω_e	2128	2201	2237	2235	2279	2353	2220	2150	2143
	R_{CO}	1.137	1.128	1.123	1.123	1.121	1.112	1.128	1.135	1.128
$[Au\text{-}CO]^+$	ω_e	2208	2282	2334	2337	2388	2481	2341	2258	2237[37]
	$\Delta\omega$	80	81	97	102	109	128	121	108	94
	R_{CO}	1.130	1.120	1.113	1.112	1.108	1.098	1.115	1.123	–
	$R_{CO\text{-}Au}$	1.896	1.924	1.927	1.979	1.982	1.940	1.954	1.934	–
	$E_{X\text{-}CO}$	2.67	2.21	2.25	1.97	1.67	1.71	1.95	2.13	–
$[L\text{-}Au\text{-}CO]^+$	ω_e	2162	2237	2289	2295	2343	2438	–	–	2192[40]
	$\Delta\omega$	34	36	52	60	64	85	–	–	49
	R_{CO}	1.14	1.125	1.118	1.117	1.113	1.102	–	–	–
	$R_{CO\text{-}Au}$	1.95	1.965	1.959	2.002	2.002	1.973	–	–	–
	$E_{X\text{-}CO}$	2.02	1.85	1.93	1.76	1.51	1.56	–	–	–
$[Au\text{-}CO]^{2+}$	ω_e	2249	2337	2401	2411	2467	2566	2391	2300	–
	$\Delta\omega$	121	136	164	176	188	213	171	150	–
	R_{CO}	1.122	1.112	1.105	1.104	1.100	1.089	1.109	1.117	–
	$R_{CO\text{-}Au}$	1.968	1.992	1.986	2.135	2.138	2.090	2.104	2.095	–
	$E_{X\text{-}CO}$	5.27	4.74	4.73	3.36	3.13	3.10	3.22	3.37	–
$[Au\text{-}CO]^{3+}$	ω_e	2172	2281	2337	2332	2426	2587	2361	–	–
	$\Delta\omega$	44	80	100	97	147	234	141	–	–
	R_{CO}	1.131	1.119	1.110	1.110	1.103	1.086	1.110	–	–
	$R_{CO\text{-}Au}$	2.033	2.037	2.005	2.040	1.979	2.154	2.118	–	–
	$E_{X\text{-}CO}$	10.62	9.80	10.52	10.10	9.90	5.12	4.30	–	–
F-Au-CO	ω_e	2114	2186	2234	2234	2285	2390	2260	2179	–
	$\Delta\omega$	− 14	− 15	− 3	− 1	6	37	40	29	–
	R_{CO}	1.146	1.136	1.128	1.127	1.122	1.111	1.127	1.136	–
	$R_{CO\text{-}Au}$	1.846	1.855	1.851	1.882	1.850	1.824	1.862	1.853	–
	$E_{X\text{-}CO}$	3.03	2.73	2.80	2.46	2.27	2.50	2.55	2.73	–
Cl-Au-CO	ω_e	2105	2179	2229	2232	2283	2385	2259	2175	2156[38]
	$\Delta\omega$	− 23	− 22	− 8	− 3	4	32	39	25	13
	R_{CO}	1.145	1.135	1.127	1.125	1.121	1.109	1.126	1.135	–
	$R_{CO\text{-}Au}$	1.879	1.889	1.887	1.924	1.896	1.870	1.899	1.888	–
	$E_{X\text{-}CO}$	2.50	2.29	2.30	2.02	1.77	1.86	2.12	2.30	–
Br-Au-CO	ω_e	2100	2172	2225	2229	2281	2384	2256	2171	2153[38]
	$\Delta\omega$	− 28	− 29	− 12	− 6	2	31	36	21	10
	R_{CO}	1.145	1.135	1.127	1.125	1.120	1.109	1.125	1.135	–
	$R_{CO\text{-}Au}$	1.889	1.902	1.898	1.937	1.911	1.882	1.914	1.901	–
	$E_{X\text{-}CO}$	2.33	2.08	2.13	1.84	1.62	1.74	1.92	2.10	–
CF_3-Au-CO	ω_e	2128	2199	2251	2255	2304	2403	2276	2200	2194[39]
	$\Delta\omega$	0	− 2	14	20	25	50	56	50	51
	R_{CO}	1.139	1.130	1.123	1.122	1.117	1.106	1.123	1.131	1.08
	$R_{CO\text{-}Au}$	1.945	1.962	1.950	2.000	1.993	1.959	1.973	1.958	1.98
	$E_{X\text{-}CO}$	1.55	1.40	1.51	0.89	1.15	0.02	1.39	1.47	–

CO stretching frequency and frequency shift, ω_e and $\Delta\omega$ in cm^{-1}, C–O and Au–CO bond distances, R_{CO} and $R_{CO\text{-}Au}$ in Å, and binding energy, $E_{X\text{-}CO}$, in eV

in $[Au\text{-}CO]^{3+}$. Here the CCSD value is $\Delta\omega = +141$ cm^{-1} (we could not converge the CCSD(T) calculations) while at the HSE06 level the shift is of $+100$ cm^{-1} only. The problem of describing the back-donation contribution in DFT calculations of Au(III) complexes has been discussed in a few recent studies by Tarantelli and coworkers [41–43].

Next we considered neutral molecules, in particular F-Au-CO, Cl-Au-CO, Br-Au-CO, and CF_3-Au-CO, where Au is in a formal + I oxidation state. Except for F-Au-CO, for the other systems experimental estimates of the shift are available. We start from F-Au-CO. Here the best estimate of $\Delta\omega$(CO) is the CCSD(T) calculation, $+29$ cm^{-1}; at the HSE06 level, however, the frequency of CO is red-shifted by -15 cm^{-1}, instead of being blue-shifted. The same effect, even more pronounced, is found for Cl-Au-CO and Br-Au-CO. In the Cl complex $\Delta\omega = +13$ cm^{-1} (exp. [37]) is nicely reproduced at the CCSD(T) level, $\Delta\omega = +25$ cm^{-1}, while it is red-shifted by -8 cm^{-1} at the HSE06 level; in the Br complex the experimental shift is $\Delta\omega = +10$ cm^{-1} [37], the CCSD(T) value is $\Delta\omega = +21$ cm^{-1}, but HSE06 gives $\Delta\omega = -12$ cm^{-1}, with opposite sign, Table 1. Not surprisingly the pure DFT values are even more red-shifted (e.g. at the PBE level $\Delta\omega = -23$ cm^{-1} for Cl-Au-CO and $\Delta\omega = -28$ cm^{-1} Br-Au-CO, Table 1.

A similar underestimate of the CO vibrational shift is found in CF_3-Au-CO where $\Delta\omega$(exp.) $= +51$ cm^{-1} [38] is well reproduced by the CCSD approach, $+56$ cm^{-1}, while the HSE06 method predicts a shift of $+14$ cm^{-1} only and PBE a $\Delta\omega = 0$ cm^{-1}. In general, significant underestimates are expected when the PBE or M06L pure functionals are adopted since these methods give an energetically too low position of the $2\pi^*$ MO of CO, with consequent excess of back donation and elongation of the C–O bond [44]. The typical error in $\Delta\omega$(CO) of PBE calculations for $Au^{\delta+}$ complexes is of about 40–50 cm^{-1}.

These numbers show that even using a hybrid functional does not guarantee a quantitative reproduction of the stretching frequency of CO adsorbed on $Au^{\delta+}$ atoms. While HSE06 (or M06) give reasonable values for charged species, both underestimate by 20–40 cm^{-1} the real shift in neutral compounds. Using higher fractions of exact exchange (M06-2X or M06-HF) does not improve the situation, Table 2.

From this analysis, since the CCSD(T) approach is not applicable to supercells and plane wave calculations, we have to rely on the PBE and eventually HSE06 calculations in order to get reliable values of the chemical shift to compare with the measured CO stretching frequencies.

3.2 Au SACs on TiO_2(101), ZrO_2(101), CeO_2(111) and $LaFeO_3$(001) Surfaces

Au atoms stabilized on four oxide surfaces will be discussed in this Section. For each oxide we considered five possible models of Au atoms on the terrace of the four oxides, Table 2: (a) the Au atom replaces an M cation in the lattice, $(Au)_{subM}$; (b) the Au atom replaces an O anion in the lattice, $(Au)_{subO}$; these two cases are equivalent to a neutral Au_1 atom adsorbed on a cation and anion vacancy, respectively; (c) an adsorbed Au atom on the most stable surface site, $(Au)_{ads}$; (d) a Au atom bound to an extra oxygen on the surface, $(AuO)_{ads}$, or (e) to two extra oxygens on the surface, $(AuO_2)_{ads}$. These two latter cases, $(AuO)_{ads}$, $(AuO_2)_{ads}$, can be seen as the result of the interaction of Au_1 with one or two hydroxyl groups, respectively, followed by H_2 formation [45]. In the presence of supported metal particles, this process is known as reverse hydrogen spillover [46].

Table 2 Adsorption energy, E_{ads} (eV), of Au single atom on oxide supports

E_{ads} (eV)	$(Au)_{subM}$	$(Au)_{subO}$	$(Au)_{ads}$
TiO_2	6.98	2.78	0.24
ZrO_2	7.10	4.38	0.95
CeO_2	6.92	2.78	1.29
$LaFeO_3$	3.31	2.11	1.57

The five species considered have different formal oxidation numbers. Since $(Au)_{subM}$ replaces a M^{4+} cation (M^{3+} for $LaFeO_3$) here Au has the highest formal oxidation state, + IV (or + III); the other extreme is that of $(Au)_{subO}$ where formally Au is negatively charged, with oxidation state -II. The third case, $(Au)_{ads}$, is that of gold in zero oxidation state, provided that no spontaneous charge transfer occurs when Au is deposited on the oxide, while in $(AuO)_{ads}$ and $(AuO_2)_{ads}$ the formal oxidation states are + I and + II, respectively, since the O atoms are bound simultaneously to Au and to the surface. In this way we cover the entire spectrum of oxidation states of Au. Of course, formal oxidation states do not necessarily reflect the real situation occurring when a Au atom is adsorbed on an oxide surface. Take for instance CeO_2. It has been shown that for $(Au)_{subO}(CeO_2)$, where Au occupies an O vacancy, one electron from the vacancy is transferred to Au which becomes Au^{-I}, and the other reduces a Ce^{4+} ion to Ce^{3+} [47]; for $(Au)_{ads}(CeO_2)$ the formal oxidation state is zero but the most stable state corresponds to a ionized Au^+ (oxidation state + I) due to the spontaneous transfer of the 6 s valence electron to a Ce ion that becomes Ce^{3+} [48].

Another problem is that the electronic nature of the Au atom can change when the CO molecule is adsorbed. On reducible oxides CO can induce an electron transfer from the Au 6 s orbital to the empty *d* or *f* orbitals of the oxide; on non-reducible oxides, such as MgO, it has been shown that Au can transfer the valence electron to the CO adsorbed molecule, with formation of a Au^+-CO^- complex [49]. In these cases, the CO molecule is not a good probe of the electronic nature of the specific site under examination.

Before considering the adsorption of CO on the Au SACs, we have compared the properties of CO adsorbed on the bare surfaces, without adsorbed Au, Table 3. In all four oxides CO is bound C-down on-top of a surface cation, Fig. 2, with a binding energy between 0.30 and 0.37 eV, indicating a similar nature of the interaction, with important electrostatic and dispersion contributions to the bonding. In all cases CO exhibits a positive vibrational shift; the smallest value is for ZrO_2, + 6 cm^{-1} in considerable underestimation of the experimental shift, + 51 cm^{-1} [50], the largest is for TiO_2, + 44 cm^{-1} (this latter value is close to the measured shift of + 33 cm^{-1} [51]). The other two oxides, CeO_2 and $LaFeO_3$, give rise to intermediate blue-shifts of CO ω_e, + 25 and + 18 cm^{-1}, respectively. The shift computed for $CeO_2(111)$, + 25 cm^{-1}, is slightly overestimated compared to the reported experimental shift of + 11 cm^{-1} at high CO coverage [52] and to other computed values obtained at a similar theoretical level (+ 9 cm^{-1} [53]); on the other hand, recent reports have clearly shown that the theoretical description of the vibrational properties of CO adsorbed on CeO_2 is challenging for conventional DFT approaches [54].

Next we consider the interaction of CO with $(Au)_{subM}$ species. As we mentioned above, here we are in the presence of a dopant, since Au replaces a cation in the lattice. The Au adsorption energy, computed with respect to a cation vacancy in the oxide and free Au_1, is extremely large, of the order of 7 eV for the non-magnetic TiO_2, ZrO_2, and CeO_2 oxides, Table 2; $LaFeO_3$ exhibits a smaller binding energy, 3.3 eV, Table 2. In all cases the Au atom carries a large positive charge, Table 3, which is smallest on $LaFeO_3$ because (a) the Au atom is not incorporated into the lattice, but adsorbed above the cation vacancy, see Fig. 3d, and (b) the Au ion is in a formal + III oxidation state instead of + IV as for the other oxides, Table 3.

When CO adsorption is considered, very different situations are found. When Au replaces Ti in TiO_2 CO binds very weakly, 0.23 eV, Table 3 and Fig. 3a. This binding is lower than that of CO on Ti^{4+} cations, so CO is not expected to interact with $(Au)_{subTi}$. A similar situation is found for ZrO_2,

Table 3 CO adsorption properties on Au SACs on $TiO_2(101)$, $ZrO_2(101)$, $CeO_2(111)$ and $LaFeO_3$ (001) surfaces. Adsorption energy, E_{ads} (eV), C–O bond length, R_{CO} (Å), C-M (M = Ti, Zr, Ce, Fe, Au) distance, R_{CM} (Å), Au Bader charge (before) and after CO adsorption, Q(Au) (|e|), harmonic CO stretching frequency scaled by 2143/2125 factor, ω_e (cm^{-1}), and frequency shift $\Delta\omega_e$ (cm^{-1}) with respect to free CO. (PBE + U results)

System	CO site	E_{ads} (eV)	R_{CO} (Å)	R_{CM} (Å)	Q(Au) (|e|)	ω_e (cm^{-1})	$\Delta\omega$ (cm^{-1})	Figures
$(TiO_2)_{60}$	Ti^{+IV}	0.34	1.138	2.47	–	2187	+ 44	2a
$(ZrO_2)_{60}$	Zr^{+IV}	0.37	1.142	2.53	–	2149	+ 6	2b
$(CeO_2)_{48}$	Ce^{+IV}	0.30	1.142	2.82	–	2168	+ 25	2c
$(LaFeO_3)_{24}$	Fe^{+III}	0.31	1.141	2.31	–	2161	+ 18	2d
$(Au)_{subTi}(Ti_{59}O_{120})$	Au^{+IV}	0.23	1.138	1.96	(1.28) 1.25	2188	+ 45	3a
$(Au)_{subZr}(Zr_{59}O_{120})$		0.29	1.144	3.57	(1.23) 1.23	2138	− 5	3b
$(Au)_{subCe}(Ce_{47}O_{96})$		CO_2 formation						3c
$(Au)_{subFe}(La_{24}Fe_{23}O_{72})$		1.24	1.153	1.86	(0.55) 0.55	2117	− 26	3d
$(Au)_{subO}$ $(Ti_{60}O_{119})$	Au^{-II}	0.40	1.152	2.10	(− 0.45) − 0.36	2062	− 81	4a
$(Au)_{subO}(Zr_{60}O_{119})$		0.57	1.162	2.09	(− 0.86) − 0.81	1980	− 163	4b
$(Au)_{subO}(Ce_{48}O_{95})$		0.18	1.155	2.29	(− 0.58) − 0.49	2038	− 105	4c
$(Au)_{subO}(La_{24}Fe_{24}O_{71})$		1.56	1.151	1.87	(− 0.11) 0.38	2101	− 42	4d
$(Au)_{ads}(TiO_2)_{60}$	Au^0	2.22	1.151	1.86	(0.42) 0.52	2096	− 47	5a
$(Au)_{ads}(ZrO_2)_{60}$		0.92	1.161	1.96	(− 0.09) 0.04	2009	− 137	5b
$(Au)_{ads}(CeO_2)_{48}$		2.64	1.153	1.87	(0.30) 0.40	2124	− 19	5c
$(Au)_{ads}(LaFeO_3)_{24}$		2.50	1.154	1.86	(0.59) 0.45	2110	− 33	5d
$(AuO)_{ads}(TiO_2)_{60}$	Au^{+I}	1.08	1.149	1.89	(0.58) 0.73	2127	− 16	6a
$(AuO)_{ads}(ZrO_2)_{60}$		1.30	1.150	1.87	(0.04) 0.45	2142	− 1	6b
$(AuO)_{ads}(CeO_2)_{48}$		1.41	1.154	1.87	(0.42) 0.47	2119	− 24	6c
$(AuO)_{ads}(LaFeO_3)_{24}$		1.61	1.146	1.90	(0.61) 0.97	2145	+ 2	6d
$(AuO_2)_{ads}(TiO_2)_{60}$	Au^{+II}	1.77	1.142	1.91	(1.06) 1.12	2172	+ 29	7a
$(AuO_2)_{ads}(ZrO_2)_{60}$		1.87	1.144	1.91	(1.00) 1.03	2159	+ 16	7b
$(AuO_2)_{ads}(CeO_2)_{48}$		1.17	1.144	1.92	(0.74) 1.01	2164	+ 21	7c
$(AuO_2)_{ads}(LaFeO_3)_{24}$		1.31	1.146	1.90	(0.76) 1.08	2153	+ 10	7d
$(AuO_2)_{ads}(LaFeO_3)_{24}$[a]		1.87	1.130	1.91	(0.89) 1.15	2167	+ 24	7d

[a]HSE06 result

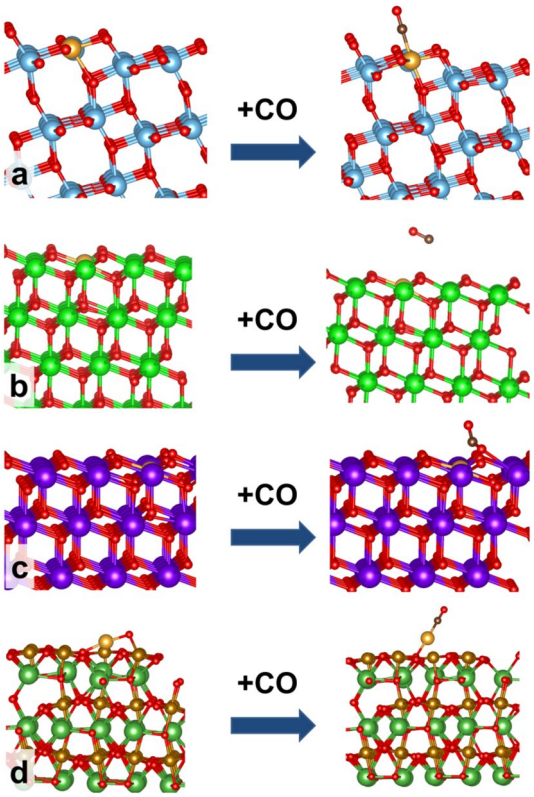

Fig. 3 CO adsorption on $(Au)_{subM}$, a Au atom substituting a lattice cation M (M = Ti, Zr, Ce, Fe) on the surface of **a** TiO_2(101), **b** ZrO_2(101), **c** CeO_2(111), and **d** $LaFeO_3$(001)

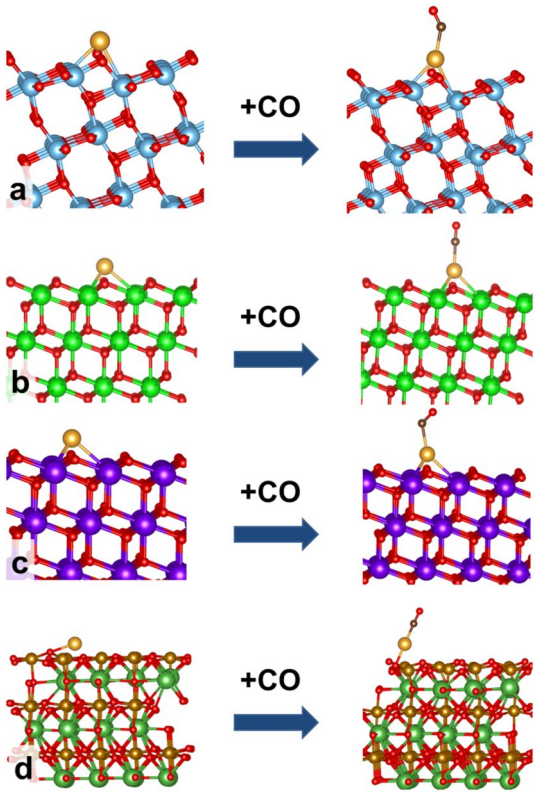

Fig. 4 CO adsorption on $(Au)_{subO}$, an Au atom replacing a lattice oxygen on the surface of **a** a-TiO_2(101), **b** ZrO_2(101), **c** CeO_2(111), and **d** $LaFeO_3$(001)

where the CO binding energy is lower than on the regular surface and the Au-CO distance is very long, Fig. 3b and Table 3. On CeO_2 the presence of a substitutional Au atom results in the destabilization of an adjacent surface oxygen so that CO reacts with this oxygen to form CO_2 that desorbs. The only oxide where CO forms a stable complex with $(Au)_{subM}$ is $LaFeO_3$, Fig. 3d. This is also the site identified as the Au SAC in the experiments performed by Tian et al. [10], so a detailed discussion of this site is required.

In the experimental study by Tian et al. [10] a CO stretching frequency of 2215 cm^{-1} was measured for a 0.3% Au loading on $LaFeO_3$ and assigned to CO adsorbed on Au SAC, Fig. 1; based on the adsorption energy of CO (DFT-PBE calculations [10]) and coordination number of Au (XANES results), it was concluded that the Au SAC on $LaFeO_3$ corresponds to the $(Au)_{subFe}$ species. Unfortunately, no DFT calculation of the CO stretching frequency has been reported. In our calculations CO is bound to $(Au)_{subFe}$ by 1.24 eV; the C–O bond length, 1.153 Å, is elongated compared to free CO and thus the CO stretching frequency is red-shifted by − 26 cm^{-1}. We have seen above that PBE overestimates the back-donation to CO, and that this negative shift is probably incorrect. However, even considering the inadequacies of the PBE functional, this is quite inconsistent with the large positive shift observed experimentally, + 72 cm^{-1}. The largest error found at the PBE level for the molecular compounds reported in Table 1 is 51 cm^{-1} (CF_3-Au-CO). Even adding this correction to the computed frequency we arrive at an estimated shift of + 25 cm^{-1}, far from the experimental value. Therefore, the assignment reported by Tian et al. does not explain the large positive shift in CO stretching frequency observed for $Au_1/LaFeO_3$. In the following we will analyze other possible Au coordination modes and provide a suggestion for an alternative assignment.

The next case is that of $(Au)_{subO}$, Tables 2, 3, and Fig. 4. Au is bound to an O vacancy of the four oxides with relatively strong bonds, from 2 to more than 4 eV, see Table 2. In all cases the Au atom is not incorporated in the surface plane, but is above it, Fig. 4, and carries a negative charge, Table 3. On $(Au)_{subO}TiO_2$, Fig. 4a, CO is bound by 0.40 eV and the CO frequency is strongly red-shifted, $\Delta\omega = -$ 81 cm^{-1}, in close agreement with previous DFT calculations on Au adsorbed on an O vacancy of rutile TiO_2 [55]; on $(Au)_{subO}ZrO_2$, Fig. 4b, the bonding is slightly stronger, 0.57 eV, and the CO frequency is significantly red-shifted, $\Delta\omega = -$ 163 cm^{-1}; on $(Au)_{subO}CeO_2$, Fig. 4c, the binding is very weak, 0.18 eV, so that no Au-CO complex is expected to form at room temperature and the adsorption site

is not competitive with the Ce ions on the surface. Finally, on $(Au)_{subO}LaFeO_3$, Fig. 4d, we have again a strong interaction, 1.56 eV, and a significant red-shift in the CO stretching frequency, $\Delta\omega = -42\ cm^{-1}$. The large red shifts observed for $(Au)_{subO}$ are not surprising and are consistent with the accumulation of negative charge and the formal -II oxidation state of gold.

The case of $(Au)_{ads}$ is the next one. Of all cases considered, this is probably the least likely. In fact, usually Au atoms adsorbed on an oxide surface are rather mobile, and tend to aggregate to form clusters, while SACs are thermally stable species. This stability can be easily explained if the Au atom replaces a lattice atom, as in the previous examples, but it is difficult to be rationalized if the atom is simply deposited on the surface. Of course, quite different interaction energies are expected as a function of the nature and morphology of the surface, and in fact for the four oxides considered in this work the adsorption energy of Au_1 goes from a minimum of 0.24 eV for TiO_2 to a maximum of 1.57 eV for $LaFeO_3$, Table 2 and Fig. 5. The other two oxides, ZrO_2 and CeO_2 have binding energies of about 1 eV, Table 2. These results are in line with previous studies: for instance, for Au atoms adsorbed on the $TiO_2(101)$ surface a value of 0.25 eV has been reported [56]; for $CeO_2(111)$ the adsorption energies are of about 1.1 eV [48, 57]. Among the four oxides considered, only $LaFeO_3$ shows an appreciable bond strength for the Au atom. Of course, what counts for the mobility of adsorbed ad-atoms is not the binding energy but the diffusion energy, which is usually much smaller [58]. Diffusion processes determine also the actual binding sites for Au atoms on oxide surfaces. For instance, for $CeO_2(111)$ it has been shown that despite a clear thermodynamic preference for oxygen vacancies, Au atoms bind mostly to regular surface sites and that even at high temperature aggregation at step edges instead of decoration of defects occurs as the consequence of adatom diffusion [59].

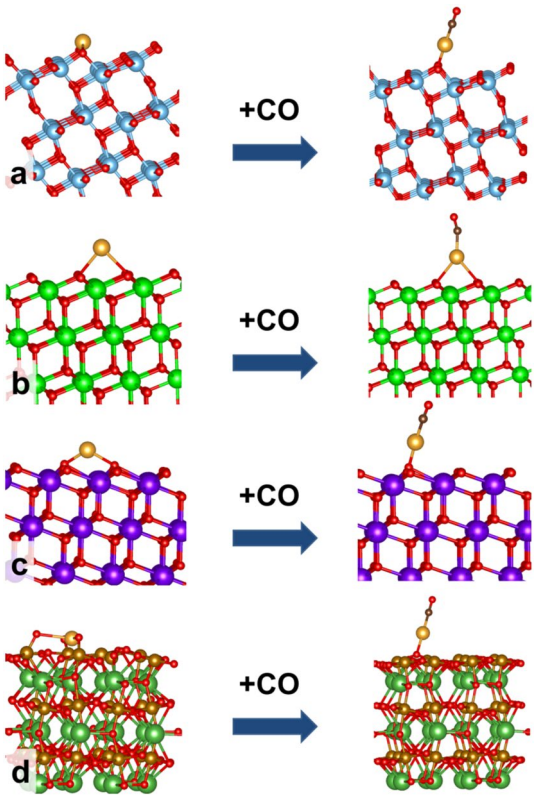

Fig. 5 CO adsorption on $(Au)_{ads}$, an Au atom bound on the surface of **a** $TiO_2(101)$, **b** $ZrO_2(101)$, **c** $CeO_2(111)$, and **d** $LaFeO_3(001)$

With the exception of zirconia, a non-reducible oxide, in all other cases Au assumes a partial positive charge as shown by the Bader charges, Table 3. This is consistent with the reducible nature of TiO_2, CeO_2, and $LaFeO_3$. Nevertheless, we consider $(Au)_{ads}$ as a case of Au atom in formally zero oxidation state. On all oxides Au is bound to the surface via the O atoms, and in $LaFeO_3$, where the interaction is stronger, two of these atoms are "extracted" from the surface to coordinate the adsorbed Au species, Fig. 5d.

CO binds rather strongly to $(Au)_{ads}$ in particular when this is supported on the three reducible oxides, TiO_2, CeO_2, and $LaFeO_3$: the Au-CO binding energy is larger than 2 eV, Table 3. This strong bonding is the consequence of the formation of a formally Au^+-CO complex, which is also consistent with the rather short Au-CO distance, about 1.86–1.87 Å, Table 3, and Fig. 5. The fact that CO adsorbed on Au_1/TiO_2 induces a charge transfer from Au to the oxide has been shown some time ago for the TiO_2 rutile surface [55]. The case of CO adsorbed on Au_1/CeO_2 has been extensively studied using methods similar to that adopted here; CO adsorption energies of 2.4–2.5 eV have been obtained for different locations of the Ce^{3+} ions with the PBE + U method [60], similar to those obtained in this study, 2.65 eV, Table 3. The case of CO adsorption on $(Au)_{ads}/ZrO_2$ is different. Here the Au atom is neutral, the Au 6 s orbital is occupied resulting in a weaker interaction with CO, 0.92 eV, and a longer Au-CO distance, 1.96 Å, Fig. 5b. This is consistent with previous DFT results [61]. In all four cases CO adsorption induces a rearrangement and change of coordination of the Au atom which is extracted from the surface plane, see Fig. 5a–d.

The different nature of the bonding in the four Au-CO surface complexes reflects in the CO stretching frequencies: on ZrO_2 the neutral Au atom gives a stronger back-donation to CO, resulting in a large negative $\Delta\omega = -137\ cm^{-1}$. Much smaller shifts are found for the other three oxides: $(Au)_{ads}/TiO_2$ $\Delta\omega = -47\ cm^{-1}$, $(Au)_{ads}/CeO_2$ $\Delta\omega = -19\ cm^{-1}$, $(Au)_{ads}/LaFeO_3$ $\Delta\omega = -33\ cm^{-1}$, Table 3. The negative shift of $-19\ cm^{-1}$ computed for $(Au)_{ads}/CeO_2$ agrees well with other theoretical estimates at the same level of theory ($\Delta\omega \approx -30\ cm^{-1}$ [60]). Also in this case, even considering

the tendency of the PBE functional to overestimate backdonation to CO, one can rule out that $(Au)_{ads}$ is the species responsible for the large positive ω shift observed experimentally for $Au_1/LaFeO_3$ [10].

We come now to two kinds of models that are quite promising since they have been proposed as the most likely structures of Rh, Ru, and Pt SACs on TiO_2 and ZrO_2 [4–9]. We are referring to the $(AuO)_{ads}$ and $(AuO_2)_{ads}$ species. We start from the former, Fig. 6. On all four oxide surfaces considered, $(AuO)_{ads}$ corresponds to an Au atom bound to two O atoms, where one is the extra oxygen on the surface, and the second is a lattice oxygen which is partly extracted from the surface, Fig. 6. On these species, where Au is in a formal + I oxidation state, Au carries a positive charge when the support is TiO_2, CeO_2, and $LaFeO_3$, Table 3; on ZrO_2 the Au atom has a Bader charge close to zero.

CO binds to $(AuO)_{ads}$ with a binding energy between 1.1 eV (TiO_2) and 1.6 eV ($LaFeO_3$), Table 3. The Au-CO distance is almost the same in all complexes, and is around 1.9 Å. After CO adsorption in all $(AuO)_{ads}$ species the positive charge on the Au atom increases, Table 3. This is because the CO molecule, that binds to Au with a σ lone pair, reinforces the electron transfer from Au to the oxide [55, 61]. Despite the positive charge on Au, which should result in a blue shift of the CO stretching frequency, the calculations indicate a CO ω_e in the range 2119–2145 cm^{-1}, i.e. slightly red-shifted or basically unchanged with respect to free CO. This is the case in particular for CO adsorbed on $(AuO)_{ads}/LaFeO_3$, where $\Delta\omega$ is + 2 cm^{-1}. Of all sites considered so far, this is the only one that gives a tiny but positive ω shift. We have mentioned already that PBE underestimates the CO ω shift by 20–50 cm^{-1}. Even considering this correction, the $(AuO)_{ads}/LaFeO_3$ species does not explain the large CO ω shift observed experimentally.

The last model of SAC considered is similar to the previous one but now the Au atom is bound to two surface O atoms instead of one, $(AuO_2)_{ads}$. The two O atoms are linked to surface cations and act as strong anchoring sites for the Au atom. They can derive from OH groups that are always present on the surface of an oxide catalyst. In some cases, e.g. TiO_2 and ZrO_2, Au is bound simultaneously to the two extra oxygens and to one oxygen from the surface, Fig. 7a, b, while in other cases it is just anchored to the two extra O atoms. Formally, in $(AuO_2)_{ads}$ Au is in a + II oxidation state and in fact the Bader charge is positive and large for all four oxides, going from + 0.74 |e| for $(AuO_2)_{ads}/CeO_2$ to + 1.06 |e| in $(AuO_2)_{ads}/TiO_2$, Table 3.

A special situation is found for the case of $LaFeO_3$ as here two iso-energetic isomers of $(AuO_2)_{ads}$ are found,

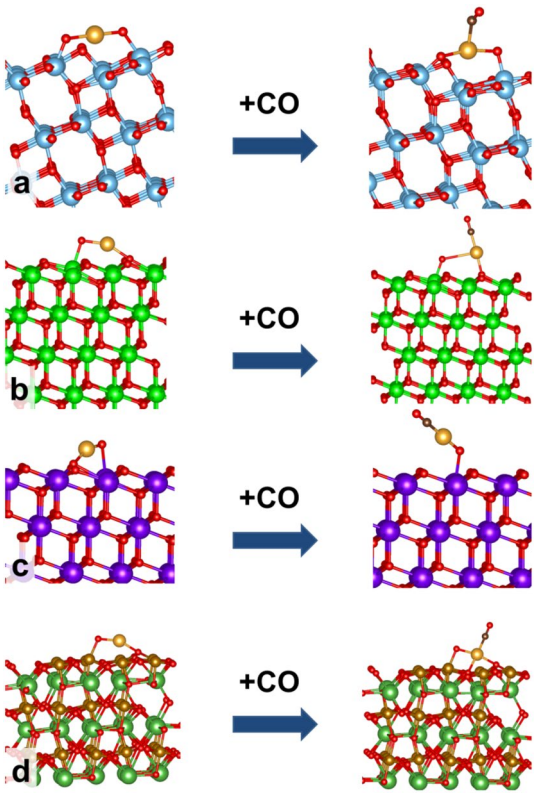

Fig. 6 CO adsorption on $(AuO)_{ads}$, a AuO complex on the surface of **a** $TiO_2(101)$, **b** r-$ZrO_2(101)$, **c** $CeO_2(111)$, and **d** $LaFeO_3(001)$

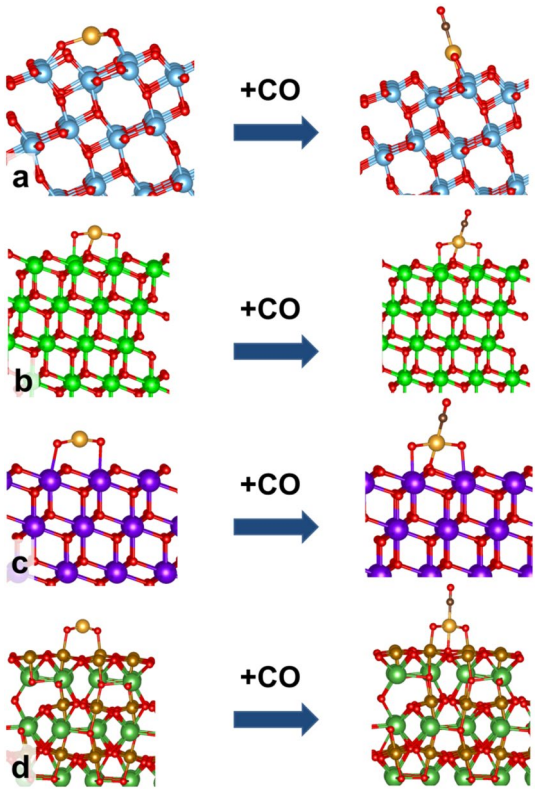

Fig. 7 CO adsorption on $(AuO_2)_{ads}$, a AuO_2 complex adsorbed on the surface of **a** $TiO_2(101)$, **b** $ZrO_2(101)$, **c** $CeO_2(111)$, and **d** $LaFeO_3(001)$

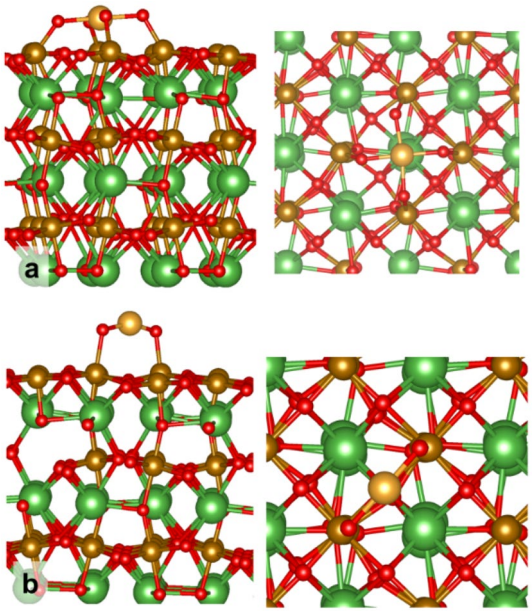

Fig. 8 Two iso-energetic structures of $(AuO_2)_{ads}$ on the surface of $LaFeO_3$(001)

Fig. 8. In the first isomer Au is bound to four O atoms, two from the $LaFeO_3$ lattice and two are the extra oxygens; this results in a square-planar coordination, Fig. 8a, where Au has similar distances from the four O atoms, 1.95–2.0 Å; the second isomer, Fig. 8b, is 0.02 eV higher in energy, and corresponds to an Au atom bound to the two extra O atoms on the surface with Au-O distances of 1.87 Å. The first structure is fully consistent with X-ray absorption near edge spectra (XANES) and X-ray absorption fine structure spectra (EXAFS) that indicate that most likely Au is bound to four O atoms with Au-O distances close to 2 Å and that Au has a positive oxidation state reminiscent of that of Au^{3+} in Au_2O_3 [10]. It is possible that the two isomers interconvert depending on the external conditions.

The adsorption of CO to $(AuO_2)_{ads}$ results in bond strengths similar to those found for $(AuO)_{ads}$, going from a minimum of 1.17 eV for $(AuO_2)_{ads}CeO_2$ to a maximum of 1.87 eV for $(AuO_2)_{ads}ZrO_2$. Again, a special situation occurs in the case of $LaFeO_3$. In fact, CO does only form a van der Waals complex on the first isomer of Fig. 8a, while is bound by 1.31 eV to the second isomer (Fig. 7d, Fig. 8b). The Au-CO distance is virtually the same in all oxides, 1.9 Å, Table 3, reflecting the very similar nature of the interaction. As it can be appreciated from the data reported in Table 3, the $(AuO_2)_{ads}$ species produces CO vibrational shifts that are positive for all four oxide surfaces: from a maximum of + 29 cm^{-1} in $(AuO_2)_{ads}TiO_2$ to a minimum of + 10 cm^{-1} for $(AuO_2)_{ads}LaFeO_3$, Table 3. These shifts are the consequence of the positive charge on Au.

Since the identification of the origin of the band at 2215 cm^{-1} in the IR spectrum of Au SAC on $LaFeO_3$ is one of the goals of this study, we decided to repeat the calculations of this specific complex using a higher level of theory. In fact, the $(AuO_2)_{ads}LaFeO_3$ species is the most promising model we have considered to explain a large Δω(CO). To this end, the calculation of the CO adsorption properties has been repeated at the HSE06 level of theory despite the considerably higher computational cost. We have seen above that the HSE06 functional provides good estimates of the CO frequency for charged $[AuCO]^{n+}$ complexes, while it underestimates the C-O stretching frequency by 20–35 cm^{-1} for neutral L-Au–CO complexes. The results are reported in the last line of Table 3. The structure of the $(AuO_2)_{ads}LaFeO_3$ complex is the same found at the PBE + U level but Δω(CO) becomes now + 24 cm^{-1}, Table 3. This is still much smaller than the + 72 cm^{-1} shift observed experimentally [10], but considering the underestimate of the HSE06 approach we can guess a computed CO shift of 40–60 cm^{-1}, not too far from the observation. While we cannot propose a firm assignment, we conclude that the $(AuO_2)_{ads}/LaFeO_3$ species is a potential candidate for the structure of the Au SAC on $LaFeO_3$.

Finally, a few words about experimental IR spectra of Au single atoms on TiO_2 and CeO_2. For Au/TiO_2 a band at 2148 cm^{-1} ($\Delta\omega = +5$ cm^{-1}) has been assigned to Au^{III} cations in the structure [51]. Of the systems studied in our work and considering the underestimate of CO ω_e by PBE, the $(AuO)_{ads}$ species seems to be the most promising. For CeO_2 frequencies in the range 2117–2150 cm^{-1} have been measured and assigned to $Au^{\delta+}(0<\delta<1)$ [62]. These frequencies are slightly below that of free CO, or just above it. They are broadly consistent with those computed here for $(Au)_{ads}CeO_2$, − 19 cm^{-1} and $(AuO)_{ads}CeO_2$, − 24 cm^{-1}.

4 Conclusions

In this paper we analyzed the possibility to identify single atom catalysts based on isolated Au atoms stabilized on an oxide support by studying the CO adsorption properties. The study of an adsorbed CO probe molecule on the Au SAC and the comparison of its vibrational frequency computed at the DFT level with experimental data can provide useful information about the site where the Au atom is stabilized. Of course, other characterization methods such as EXAFS, XANES, or TPD do also provide relevant information but here the main focus is on the CO vibrational frequency. This property is very sensitive to the oxidation state and coordination of a metal atom [63] and provides important information about the nature of the active site. The work is stimulated by a recently reported case of Au SAC on a perovskite, $LaFeO_3$, where a very high frequency has been measured for CO on

the Au species, 2215 cm^{-1}, with a blue shift of + 72 cm^{-1} compared to free CO [10]. This large blue-shift is usually due to the bonding of CO to cationic species, suggesting that Au must be in a positive oxidation state [63].

The first step of the work consisted in the assessment of the accuracy of the method used, based on a pure DFT functional, PBE. This is known to produce an overestimate of the back-donation contribution from metals to CO which, in turns, is due to a too small HOMO–LUMO gap in the free CO molecule at this level of theory [44]. This problem can be overcome using hybrid functionals, where a portion of exact exchange is included in the functional [64]. Among various formulations, here we have adopted the popular and successful HSE06 hybrid functional. To test the reliability of our computed CO stretching frequencies for $Au^{\delta+}$-CO complexes we have selected a few neutral and charged molecules containing this bond and we have computed the electronic and vibrational properties at various level of theory. Beside PBE and HSE06, also the Minnesota functionals, M06, pure and hybrid, have been tested together with the accurate and computationally demanding CCSD and CCSD(T) quantum chemical methods. The results show that while the HSE06 functional performs well in reproducing the CO frequencies of charged Au complexes, it underestimates, by 20–30 cm^{-1}, this property in neutral $Au^{\delta+}$-containing molecules. The underestimate is of course larger in the case of the PBE functional, 20–50 cm^{-1}.

Having established the error bar that should be expected in the calculation of the CO stretching frequency for Au on oxide surface, we have considered five possible structural motifs of Au SACs on four supports: anatase TiO_2, tetragonal ZrO_2, cubic CeO_2, and perovskite $LaFeO_3$. The sites considered are: (a) an Au atom that replaces a M cation in the lattice, $(Au)_{subM}$; (b) an Au atom that replaces an O anion in the lattice, $(Au)_{subO}$; (c) an Au atom adsorbed on the surface, $(Au)_{ads}$; (d) an Au atom bound to an extra oxygen on the surface, $(AuO)_{ads}$; (e) an Au atom bound to two extra oxygens on the surface, $(AuO_2)_{ads}$. These two latter cases, $(AuO)_{ads}$, $(AuO_2)_{ads}$, can be the result of the interaction of Au with hydroxyl groups present on the surface. All systems considered are charge neutral.

Most of the sites considered give rise to strong or significant red-shifts in the CO ω_e; even considering the limitations of the PBE approach, it is possible to rule out $(Au)_{subM}$, $(Au)_{subO}$, and $(Au)_{ads}$ as the species that give rise to a large blue-shift in CO ω_e in $Au_1/LaFeO_3$. Only the $(AuO_2)_{ads}$ species exhibits significant positive shifts. Taking into account the underestimate of the PBE and HSE06 methods, one can guess a CO ω_e for $(AuO_2)_{ads}LaFeO_3$ close to that observed experimentally [10]. While this is not sufficient to propose a firm assignment, it represents a possible explanation of the IR spectra not considered so far. The results also show the large number of potential sites occupied by SACs and point to the need to fully characterize them structurally if one is interested in the calculation with electronic structure methods of the chemical and catalytic properties of a SAC.

Acknowledgements Open access funding provided by Università degli Studi di Milano—Bicocca within the CRUI-CARE Agreement.

Funding Open access funding provided by Università degli Studi di Milano - Bicocca within the CRUI-CARE Agreement. Funding was provided by Ministero dell'Istruzione, dell'Università e della Ricerca (Grant No. 20179337R7 MULTI-e). This research is funded by Vietnam National Foundation for Science and Technology Development (NAFOSTED) under grant number 104.06-2020.50.

Declarations

Conflict of interest The authors declare no conflict of interest.

Research Involving Human and Animal Participants This research does not involve experiments on animals or humans.

References

1. Wang A, Li J, Zhang T (2018) Heterogeneous single-atom catalysis. Nature Rev Chem 2:65–81
2. Yang XF, Wang A, Qiao B, Li J, Liu J, Zhang T (2013) Single-atom catalysts: a new frontier in heterogeneous catalysis. Acc Chem Res 46:1740–1748
3. Samantaray MK, D'Elia V, Pump E, Falivene L, Harb M, Chikh SO, Cavallo L, Basset JM (2020) The comparison between single atom catalysis and surface organometallic catalysis. Chem Rev 120:734–813
4. Rita LD, Resasco J, Dai S, Boubnov A, Thang HV, Hoffman AS, Ro I, Graham GW, Bare SR, Pacchioni G, Pan X, Christopher P (2019) Structural evolution of atomically dispersed Pt catalysts dictates reactivity. Nat Mater 18:746–751
5. Thang HV, Pacchioni G, Rita LD, Christopher P (2018) Nature of stable single atom Pt catalysts dispersed on anatase TiO2. J Catal 367:104–114
6. Thang HV, Tosoni S, Fang L, Bruijnincx P, Pacchioni G (2018) Nature of sintering-resistant, single-atom Ru species dispersed on zirconia-based catalysts: a DFT and FTIR study of CO adsorption. ChemCatChem 10:2634–2645
7. Thang HV, Pacchioni G (2019) Nature of atomically dispersed Ru on anatase TiO2: revisiting old data based on DFT calculations. J Phy Chem C 123:7271–7282

8. Thang HV, Pacchioni G (2020) On the real nature of Rh single-atom catalysts dispersed on the ZrO2 surface. ChemCatChem 12:2595–2604
9. Asokan C, Thang HV, Pacchioni G, Christopher P (2020) Reductant composition influences the coordination of atomically dispersed Rh on anatase TiO2. Catal Sci Technol 10:1597–1601
10. Tian C et al (2020) A new trick for an old support: stabilizing gold single atoms on LaFeO3 perovskite. Appl Catal B 261:118178
11. Frisch MJ, Trucks GW, Schlegel HB, Scuseria GE, Robb MA, Cheeseman JR, Scalmani G, Barone V, Petersson GA, Nakatsuji H, Li X, Caricato M, Marenich AV, Bloino J, Janesko BG, Gomperts R, Mennucci B, Hratchian HP, Ortiz JV, Izmaylov AF, Sonnenberg JL, Williams-Young D, Ding F, Lipparini F, Egidi F, Goings J, Peng B, Petrone B, Henderson T, Ranasinghe D, Zakrzewski VG, Gao J, Rega N, Zheng G, Liang W, Hada M, Ehara M, Toyota K, Fukuda R, Hasegawa J, Ishida M, Nakajima T, Honda Y, Kitao O, Nakai H, Vreven T, Throssell K, Montgomery JA, Peralta JJE, Ogliaro F, Bearpark MJ, Heyd JJ, Brothers EN, Kudin KN, Staroverov VN, Keith TA, Kobayashi R, Normand J, Raghavachari K, Rendell AP, Burant JC, Iyengar SS, Tomasi J, Cossi M, Millam JM, Klene M, Adamo C, Cammi R, Ochterski JW, Martin RL, Morokuma K, Farkas O, Foresman JB, Fox DJ (2016) Gaussian 16, revision A.03. Gaussian Inc., Wallingford
12. Kresse G, Furthmüller J (1996) Efficiency of ab-initio total energy calculations for metals and semiconductors using a plane-wave basis set J. Comput Mater Sci 6:15–50
13. Rappoporta D, Furche F (2010) Property-optimized Gaussian basis sets for molecular response calculations. J Chem Phys 133:134105
14. Andrae D, Häußermann U, Dolg M, Stoll H, Preuß H (1990) Energy-adjustedab initio pseudopotentials for the second and third row. Theor Chim Acta 77:123–141
15. Perdew J, Burke K, Ernzerhof M (1996) Generalized gradient approximation made simple. Phys Rev Lett 77:3865
16. Zhao Y, Truhlar DJ (2006) A new local density functional for main-group thermochemistry, transition metal bonding, thermochemical kinetics, and noncovalent interactions. J Chem Phys 125:194101
17. Heyd J, Scuseria GE, Ernzerhof M (2006) Erratum: hybrid functionals based on a screened coulomb potential. J Chem Phys 124:219906
18. Zhao Y, Truhlar DG (2008) The M06 suite of density functionals for main group thermochemistry, thermochemical kinetics, noncovalent interactions, excited states, and transition elements: two new functionals and systematic testing of four M06-class functionals and 12 other functionals. Theor Chem Acc 120(1–3):215–241
19. ZhaoY TDG (2006) Density functional for spectroscopy: no long-range self-interaction error, good performance for Rydberg and charge-transfer states, and better performance on average than B3LYP for ground states. J Phys Chem A 110(49):13126–13130
20. Shavitt I, Bartlett RJ (2009) Many-body methods in chemistry and physics: MBPT and coupled-cluster theory. Cambridge University Press, Cambridge
21. Blöchl PE (1994) Projector augmented-wave method. Phys Rev B 50:17953
22. Kresse G, Joubert J (1999) From ultrasoft pseudopotentials to the projector augmented-wave method. Phys Rev B 59:1758
23. Han Y-K, Hirao K (2000) On the transferability of relativistic pseudopotentials in density-functional calculations: AuH, AuCl and Au2. Chem Phys Lett 324:453
24. Zhang L, Filot IAW, Su YQ, Liu JX, Hensen EJM (2019) Understanding the impact of defects on catalytic CO oxidation of LaFeO3 supported Rh, Pd and Pt single atom catalysts. J Phys Chem C 123:290–7298
25. Huang M, Fabris S (2008) CO adsorption and oxidation on ceria surfaces from DFT+U calculations. J Phys Chem C 112(23):8643–8648
26. Chen HYT, Tosoni S, Pacchioni G (2015) Adsorption of ruthenium atoms and clusters on anatase TiO2 and tetragonal ZrO2(101) surfaces: a comparative DFT study. J Phys Chem C 119:10856
27. Taylor FH, Buckeridge J, Catlow CRA (2016) Defects and oxide ion migration in the solid oxide fuel cell cathode material LaFeO3. Chem Mater 28:8210–8220
28. Marezio M, Dernier PD (1971) The bond lengths in LaFeO3. Mat Res Bull 6:23–30
29. Zhang Q, Huang Y, Peng S, Zhang Y, Shen Z, Cao ZJ, Ho W, Lee SC, Pui AYH (2017) Perovskite LaFeO3-SrTiO3 composite for synergistically enhanced NO removal under visible light excitation. Appl Catal B 204:346–357
30. Sarma DD, Shanthi N, Barman SR, Hamada N, Sawada H, Terakura K (1995) Band theory for ground-state properties and excitation spectra of perovskite LaMO3 (M = Mn, Fe Co, Ni). Phys Rev Lett 75:1126
31. KoehlerWC WEO (1957) Neutron-diffraction study of the magnetic properties of perovskite-like compounds LaBO3. J Phys Chem Solids 2:100–106
32. Tang W, Sanville E, Henkelman G (2009) A grid-based bader analysis algorithm without lattice bias. J Phys Condens Matter 21:084204
33. Henkelman G, Arnaldsson A, Jónsson H (2006) A fast and robust algorithm for bader decomposition of charge density. Comput Mater Sci 36:254–360
34. Yu M, Trinkle DR (2011) Accurate and efficient algorithm for bader charge integration. J Chem Phys 134:064111
35. Blanck D, Berrier E, Paul JF (2017) First-principles investigation of the relevant surfaces exposed by polycrystalline LaFeO3. ChemCatChem 9:2383–2389
36. Liang B, Andrews L (2000) Reactions of laser-ablated Ag and Au atoms with carbon monoxide: matrix infrared spectra and density functional calculations on Ag(CO)n (n = 2, 3), Au(CO)n (n = 1, 2) and M(CO)n+ (n = 1–4; M = Ag, Au). J Phys Chem A 104(40):9156–9164
37. Dell'Amico DB, Calderazzo F, Robino P, Segre A (1991) Halogenocarbonyl complexes of gold. J Chem Soc Dalton Trans 11:3017–3020
38. Martínez-Salvador S, Forniés J, Martín A, Menjón B (2011) [Au(CF3)(CO)]: a gold carbonyl compound stabilized by a trifluoromethyl group. Angew Chem Int Ed 50:6571–6574
39. Dash C, Kroll P, Yousufuddin M, Dias HVR (2011) Isolable, gold carbonyl complexes supported by N-heterocyclic carbenes. Chem Commun 47:4478–4480
40. Tielens F, Garcia L, Polo V, Andres J (2007) A theoretical study on the electronic structure of Au-XO(0,-1,+1) (X = C, N, O). J Phys Chem A 111:13255
41. Bistoni G, Rampino S, Scafuri N, Ciancaleoni G, Zuccaccia D, Belpassi L, Tarantelli F (2016) How π back-donation quantitatively controls the CO stretching response in classical and non-classical metal carbonyl complexes. Chem Sci 7(2):1174–1184
42. Sorbelli D, Belpassi L, Tarantelli F, Belanzoni P (2018) Ligand effect on bonding in gold (III) carbonyl complexes. Inorg chem 57(10):6161–6175
43. Gaggioli CA, Belpassi L, Tarantelli F, Belanzoni P (2017) The gold (iii)–CO bond: a missing piece in the gold carbonyl complex landscape. Chem Comm 53(10):1603–1606
44. Gil A, Clotet A, Ricart JM, Kresse G, Garcıa-Hernández M, Rösch N, Sautet P (2003) Site preference of CO chemisorbed on Pt (1 1 1) from density functional calculations. Surf Sci 530(1–2):71–87

45. Schlexer P, Pacchioni G (2017) Adsorption and dimerization of late transition metal atoms on the regular and defective quartz (001) surface. Top Catal 60:459–470
46. Vayssilov GN, Rösch N (2005) Reverse hydrogen spillover in supported subnanosize clusters of the metals of groups 8 to 11. A computational model study. Phys Chem Chem Phys 7:4019–4026
47. Penschke C, Paier J (2017) Reduction and oxidation of Au adatoms on the CeO2 (111) surface–DFT+ U versus hybrid functionals. Phys Chem Chem Phys 19(19):12546–12558
48. Zhang C, Michaelides A, King DA, Jenkins SJ (2008) Structure of gold atoms on stoichiometric and defective ceria surfaces. J Chem Phys 129(19):194708
49. Sterrer M, Yulikov M, Risse T, Freund HJ, Carrasco J, Illas F, Di Valentin C, Gordano L, Pacchioni G (2006) When the reporter induces the effect: unusual IR spectra of CO on Au1/MgO(001)/Mo(001). Angew Chem Int Ed 45(16):2633–2635
50. Bolis V, Morterra C, Fubini B, Ugliengo P, Garrone E (1993) Temkin-type model for the description of induced heterogeneity: CO adsorption on group 4 transition metal dioxides. Langmuir 9:1521–1528
51. Boronat M, Concepción P, Corma A (2009) Unravelling the nature of gold surface sites by combining IR spectroscopy and DFT calculations. Implications in catalysis. J Phys Chem C 113(38):16772–16784
52. Yang C, Yin LL, Bebensee F, Buchholz M, Sezen H, Heissler S, Chen J, Nefedov A, Idriss H, Gong XQ, Wöll C (2014) Chemical activity of oxygen vacancies on ceria: a combined experimental and theoretical study on CeO2 (111). Phys Chem Chem Phys 16(44):24165–24168
53. Yang C, Yu X, Heißler S, Weidler PG, Nefedov A, Wang Y, Wöll C, Kropp T, Paier J, Sauer J (2017) O2 activation on ceria catalysts—the importance of substrate crystallographic orientation. Angew Chem Int Ed 56:16399
54. Lustemberg PG, Plessow PN, Wang Y, Yang C, Nefedov A, Studt F, Wöll C, Ganduglia-Pirovano MV (2020) Vibrational frequencies of cerium-oxide-bound CO: a challenge for conventional DFT methods. Phys Rev Lett 125:256101
55. Wörz AS, Heiz U, Cinquini F, Pacchioni G (2005) Charging of Au atoms on TiO2 thin films from CO vibrational spectroscopy and DFT calculations. J Phys Chem B 109(39):18418–18426
56. Gong XQ, Selloni A, Dulub O, Jacobson P, Diebold U (2008) Small Au and Pt clusters at the anatase TiO2 (101) surface: behavior at terraces, steps, and surface oxygen vacancies. J Am Chem Soc 130:370–381
57. Hernandez NC, Grau-Crespo R, de Leeuw NH, Sanz JF (2009) Electronic charge transfer between ceria surfaces and gold adatoms: a GGA+U investigation. Phys Chem Chem Phys 11:5246–5252
58. Tosoni S, Pacchioni G (2017) Influence of surface hydroxylation on the Ru atom diffusion on the ZrO2(101) surface: a DFT study. Surf Sci 664:87–94
59. Lustemberg PG, Pan Y, Shaw BJ, Grinter D, Pang C, Thornton G, Pérez R, Ganduglia-Pirovano MV, Nilius N (2016) Diffusion barriers block defect occupation on reduced CeO2 (111). Phys Rev Lett 116:236101
60. Schilling C, Ziemba M, Hess C, Ganduglia-Pirovano MV (2020) Identification of single-atom active sites in CO oxidation over oxide-supported Au catalysts. J Catal 383:264–272
61. Puigdollers AR, Illas F, Pacchioni G (2016) Effect of nanostructuring on the reactivity of zirconia: a DFT+U study of Au atom adsorption. J Phys Chem C 120(31):17604–17612
62. Wu Z, Jiang DE, Mann AKP, Mullins R, Qiao ZA, Allard LF, Zeng C, Jin R, Overbury SH (2014) Thiolate ligands as a double-ddged sword for CO oxidation on CeO2 supported Au25(SCH2CH2Ph)18 nanoclusters. J Am Chem Soc 136(16):6111–6122
63. Pacchioni G, Cogliandro G, Bagus PS (1992) Molecular orbital cluster model study of bonding and vibrations of CO adsorbed on MgO surface. Int J Quantum Chem 42:1115–1139
64. Tosoni S, Li C, Schlexer P, Pacchioni G (2017) CO adsorption on graphite-like ZnO bilayers supported on Cu(111), Ag(111) and Au(111) surfaces. J Phys Chem C 121:27453–27461